Scintigraphic Evaluation of Pancreatic Transplants Using Technetium-99m-Sestamibi

Abdelhamid H. Elgazzar, Rino Munda, Mariano Fernandez-Ulloa, James Clark, Janet R. Ryan and Judy A. Hughes

Division of Nuclear Medicine, Departments of Radiology and Surgery, University of Cincinnati Hospital, Cincinnati, Ohio

The purpose of this study was to evaluate the feasibility of using ^{99m}Tc-sestamibi in the assessment of pancreatic transplant. **Methods:** Ten transplant recipients with a history of insulin-dependent diabetes mellitus were studied. Fourteen ^{99m}Tc-sestamibi studies were performed. Each patient was injected intravenously with 10 mCi of ^{99m}Tc-sestamibi. Two-second frames were obtained for 1 min, followed by serial dynamic and static images every 5 min for 30 min. Technetium-99m sestamibi studies, read by two nuclear medicine physicians, were correlated with clinicopathologic findings and compared to the ten ^{201}Tl studies obtained in seven of these patients. **Results:** On ^{99m}Tc-sestamibi images, normally functioning grafts showed adequate perfusion on the angiogram and good uptake followed by clearance on static images. Time-activity curves showed an initial upslope followed by a downslope after the initial uptake peak. The quality of ^{99m}Tc-sestamibi images was superior to those of ^{201}Tl in five, similar in four and marginally inferior in one paired study. Technetium-99m-sestamibi was used for both flow and static images, whereas a ^{99m}Tc radiotracer angiogram was needed to accompany the ^{201}Tl study. **Conclusion:** Our preliminary experience indicates that ^{99m}Tc-sestamibi helps evaluate pancreatic transplants and provides high count statistics, which result in better image quality and diagnostic detail. Extensive quantitative studies are being performed to further evaluate this agent's role in the clinical management of pancreatic transplant patients.

Key Words: pancreatic transplantation; scintigraphy; technetium-99m-sestamibi; thallium-201

J Nucl Med 1995; 36:771–777

Pancreatic transplantation is being used with increasing frequency as a safe, effective therapeutic option for patients with insulin-dependent diabetes mellitus. Improvement in microvascular and neuropathic complications of diabetes and an increase in psychological wellbeing have been noted following such transplantation (*1,2*). Currently, renal and pancreatic transplants are often performed simultaneously in patients with end-stage renal disease caused by insulin-dependent diabetes mellitus. Both organs are obtained from the same donor. Parameters used for evaluation of renal transplant rejection have been used as indirect indicators for pancreatic transplant rejection (*3–5*). Renal and pancreatic rejection, however, can occur discordantly (*6,7*). Additionally, solitary pancreatic transplantation without simultaneous renal transplantation is occasionally performed in nonuremic diabetics (*8*).

Pancreatic transplants have been evaluated by serum glucose, amylase and lipase levels, insulin requirements and urine amylase in patients in whom the exocrine secretions drain into the urinary bladder (*9*). These parameters, however, are nonspecific for the cause of decreased function (*10*). Pancreatic biopsy is rarely performed due to the risk of serious complications (*11*). An independent imaging method for evaluation of pancreatic transplants would be valuable (*12*) to detect the common posttransplant complications including rejection, which can be difficult to diagnose (*2*). Several imaging modalities have been tried for pancreatic transplant evaluation, including US, CT, MRI and other scintigraphic methods (*11–24*). Yet, none of these are ideal for evaluating transplant complications because of inadequate specificity. In an attempt to find a suitable radiotracer for pancreatic transplantation, ^{201}Tl has been used recently to evaluate pancreatic grafts. Thallium-201 images, however, have to be interpreted in conjunction with a ^{99m}Tc flow study for proper evaluation of the vascularity and viability of the graft (*23*). Technetium-99m-sestamibi has been introduced as a myocardial imaging agent. It has also been used in the detection of abnormal parathyroid glands and a variety of viable tumors. To establish the possible use of ^{99m}Tc-sestamibi in evaluating the vascularity and viability of pancreatic transplants, we correlated the patterns of flow and uptake of this agent with clinicopathologic data and with ^{201}Tl images obtained from some of the patients.

MATERIALS AND METHODS

Patients

Ten patients with a history of insulin-dependent diabetes mellitus and end-stage renal disease were studied. There were six females and four males, ages 28 to 47 yr. Each patient had received a renal and pancreatic graft simultaneously from a brain dead, heart-beating donor. Grafts were placed in the iliac fossae.

Received Aug. 31, 1994; revision accepted Jan. 3, 1994.

For correspondence or reprints contact: Abdelhamid H. Elgazzar, MD, Division of Nuclear Medicine, Department of Radiology, Mt. Sinai School of Medicine, One Gustave Levy Pl., New York, NY 10029-6574.

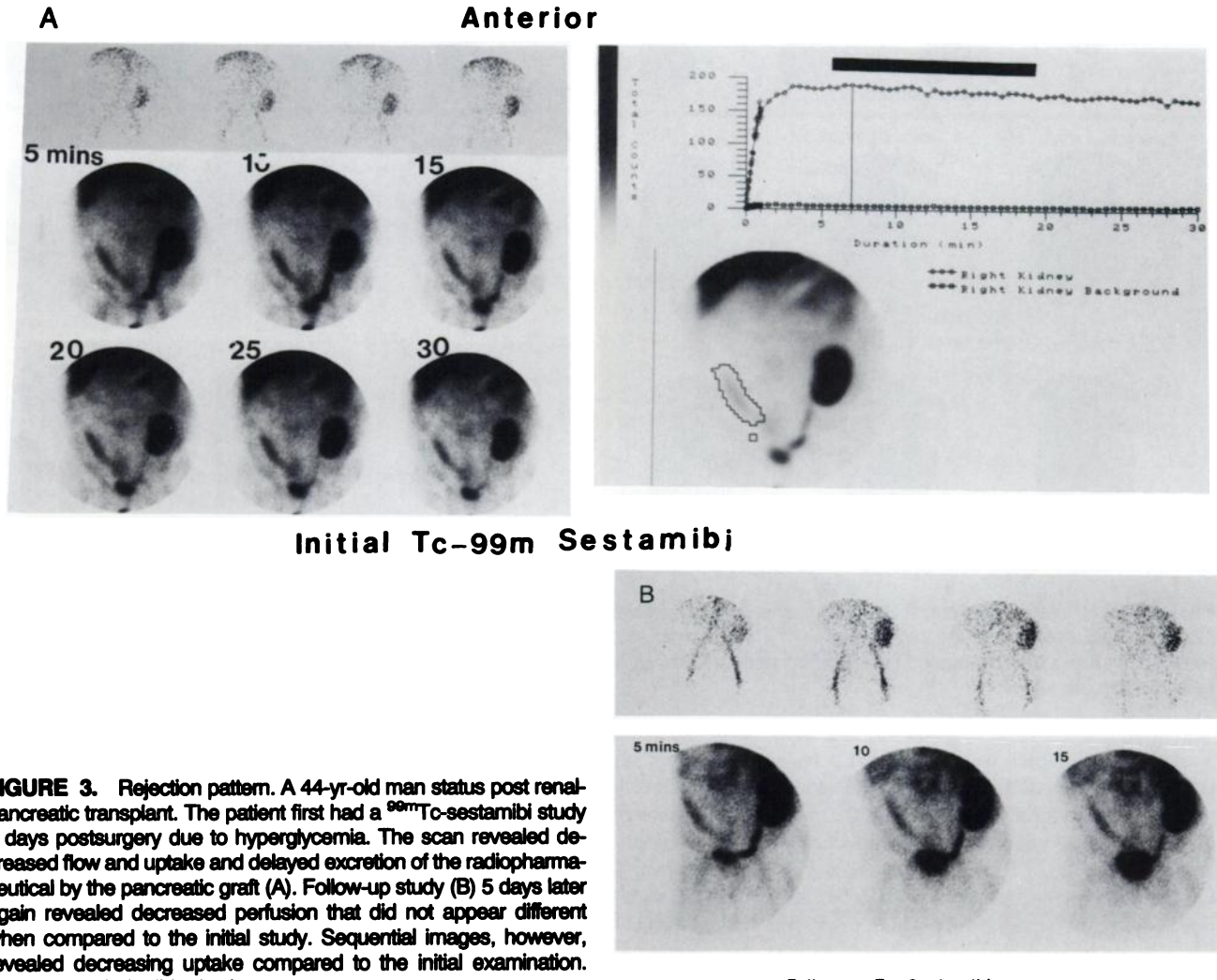

FIGURE 3. Rejection pattern. A 44-yr-old man status post renal-pancreatic transplant. The patient first had a ^{99m}Tc-sestamibi study 7 days postsurgery due to hyperglycemia. The scan revealed decreased flow and uptake and delayed excretion of the radiopharmaceutical by the pancreatic graft (A). Follow-up study (B) 5 days later again revealed decreased perfusion that did not appear different when compared to the initial study. Sequential images, however, revealed decreasing uptake compared to the initial examination. Biopsy revealed mild rejection.

sestamibi static images were found to be of better quality with better delineation of the grafts than on ^{201}Tl images.

One patient who showed good function initially later developed pancreatitis. The ^{99m}Tc-sestamibi flow study showed good flow to the transplant, and static images revealed poor visualization and retention of activity (Fig. 4). In the remaining patient, the ^{99m}Tc-sestamibi study revealed absent flow and uptake (a photon-deficient area) at the site of the transplant on the right iliac fossa. This patient proved to have venous thrombosis, and the graft was later removed (Fig. 5).

Several scintigraphic patterns were identified:

1. Normal pattern (three patients). Angiogram with peak pancreatic activity less than 6 sec from arterial peak and equal graft to arterial intensity as well as homogeneous uptake by the pancreatic transplant with good graft definition on static images.
2. Rejection pattern (five patients). Early rejection was manifested by decreased flow with a less- apparent degree of decreased uptake on static images; later images revealed further decreased uptake. Inhomogeneous uptake and retention of activity on static images was also seen. Progressive decrease of flow and/or uptake on serial images indicated the diagnosis. In one case of rejection, decreasing uptake on serial images was easier to identify than perfusion differences on flow images.
3. Pancreatitis pattern (one patient). Good perfusion on the angiogram with decreased uptake on static images was noted in one case of pancreatitis. Apparent retention of activity on static images was also noted.
4. Vascular thrombosis (one patient). Absent flow and uptake with a photon-deficient area at the site of the graft.

Among patients who had both ^{99m}Tc and ^{201}Tl studies, the overall quality of ^{99m}Tc-sestamibi was superior to ^{201}Tl in five, similar in four, and borderline inferior in one of the ten paired studies. Technetium-99m-sestamibi was used for both flow and static images in contrast to ^{201}Tl, which had to be combined with a ^{99m}Tc radiotracer angiogram for evaluation of vascularity and graft viability.

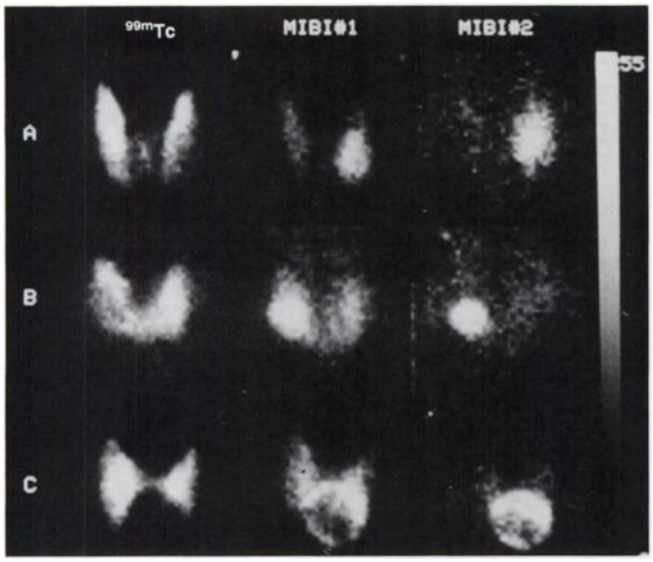

FIGURE 1. Scintigraphs of three representative Group A patients show intense, persistent deposition of MIBI on a cold nodule.

tissue; 3 = uptake in the nodule superior to that of the thyroidal tissue.

Scintigraphic Data Processing

The early and late images were expanded over 256 × 256 matrices and displayed together. Squared regions of interest (ROIs) (16 × 16 pixels) were drawn over the nodule, normal thyroid tissue and surrounding extrathyroidal tissue. The location of regions was identical for both images. After background subtraction, the counts in the nodule and extranodular tissue were normalized for acquisition time and ^{99m}Tc decay. The nodular-to-extranodular normal thyroidal tissue (N/T) ratio was calculated for early and late images and the washout rate (fraction of the tracer removed) from the nodule (WON) and the extranodular normal thyroidal tissue (WOT) was also calculated and expressed as hr^{-1}. Mann-Whitney (between groups) and Wilcoxon signed-rank (within groups) tests were used for statistical analysis.

Histopathologic Data Analysis

Since some patients underwent surgery at different hospitals, surgical specimens from these patients were collected for pathologic analysis. The pathologist was first asked to diagnose the lesion and then score the percentage of oxyphilic cells compared to whole cellularity.

RESULTS

Visual Inspection

In the early study, 23 patients exhibited clear nodular MIBI uptake (score 1, 2, 3). On the late studies, eight patients (Group A) showed persistent nodular uptake and washout in thyroid tissue (score 3), whereas 15 patients (Group B) showed nodular and thyroid tissue washout (score 0).

The average scores in the early study for Groups A and B were 2.75 ± 0.46 and 1.73 ± 0.88 ($p < 0.01$) and 3.00 ± 0.00 and 0.00 for late studies ($p < 0.001$). A statistically significant difference was found in Group B between early and late studies ($p < 0.001$). No statistical difference was noticed in Group A between early and late studies. The remaining 18 patients (Group C) did not show significant nodular MIBI uptake in the early study (score 0) and had no scintigraphic data processing.

Scintigraphic Data

Uptake Ratio. The early N/T ratio were 1.77 ± 0.46 and 1.45 ± 0.54 (p = ns); the late ones were 3.20 ± 1.37 and 0.84 ± 0.30 ($p < 0.0001$) for Groups A and B, respectively. The differences between early and late studies were statistically significant in both groups (A: $p < 0.01$; B: $p < 0.001$).

Washout Rate. WON was 17.2 ± 6.3 and 30.0 ± 7.3 ($p < 0.001$) and WOT was 24.6 ± 7.5 and 24.5 ± 6.8 (p = ns) for Groups A and B, respectively. A statistically

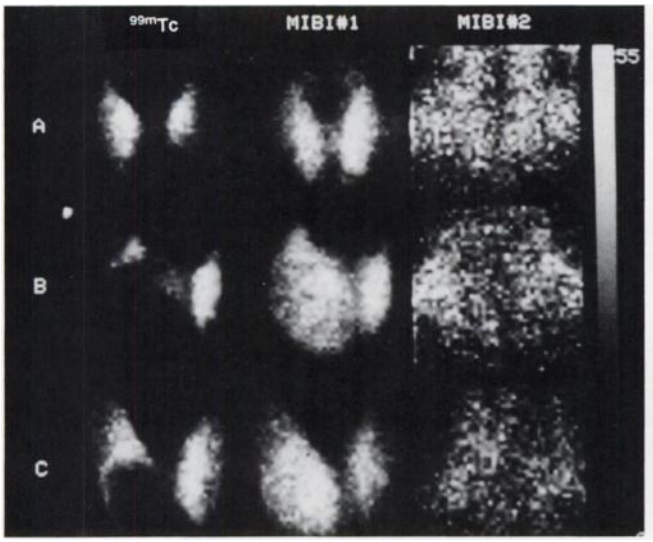

FIGURE 2. Scintigraphs of three representative Group B patients show intense MIBI uptake with fading activity on a cold nodule.

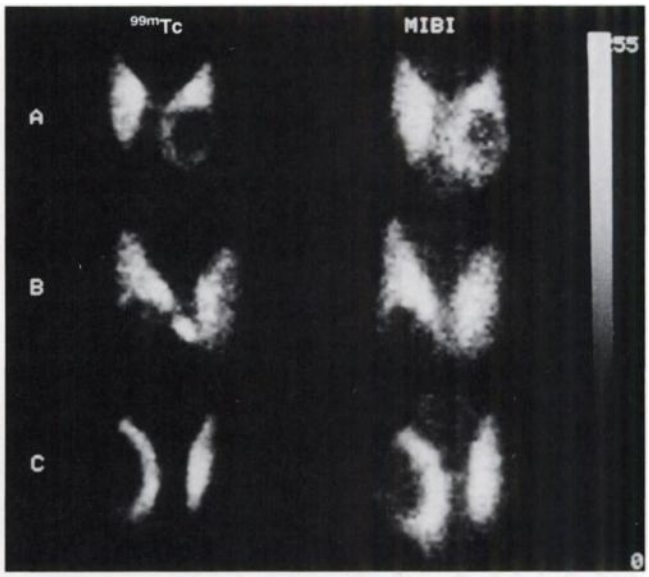

FIGURE 3. Scintigraphs of three representative Group C patients show no MIBI uptake on a cold nodule.

TABLE 1
Individual Scintigraphic Results

Patient no.	N/T ratio		Washout rate (hr^{-1})		Score	
	Early	Late	N	T	Early	Late
Group A						
1*	1.69	2.81	11.2%	19.0%	3	3
2*	2.39	6.01	15.4%	23.3%	3	3
3*	1.14	1.80	17.6%	22.0%	2	3
4*	1.78	3.26	9.9%	23.4%	3	3
5*	2.41	2.91	12.5%	15.1%	3	3
6	1.79	2.86	19.8%	24.0%	3	3
7	1.74	4.16	23.2%	39.8%	3	3
8	1.23	1.77	28.3%	30.1%	2	3
mean ± s.d.	1.77 ± 0.46	3.20 ± 1.37	17.2% ± 6.3%	24.6% ± 7.5%	2.75 ± 0.46	3.00 ± 0.00
Group B						
9*	0.94	0.81	27.9%	26.9%	1	0
10*	1.00	0.93	23.1%	22.4%	1	0
11*	1.72	0.71	21.8%	17.8%	2	0
12*	1.68	1.07	33.1%	30.1%	2	0
13*	0.99	0.80	31.7%	27.8%	1	0
14*	2.21	0.58	43.6%	33.3%	3	0
15*	0.82	0.65	21.7%	20.8%	1	0
16*	1.41	0.48	39.3%	29.1%	1	0
17*	1.82	1.35	32.8%	13.7%	2	0
18*	2.13	1.56	32.5%	29.7%	3	0
19	2.22	0.65	20.2%	15.4%	3	0
20	0.84	0.89	22.5%	23.1%	1	0
21	0.70	0.63	34.9%	32.8%	1	0
22	1.33	0.61	26.3%	14.6%	1	0
23	1.87	0.90	38.0%	30.7%	3	0
mean ± s.d.	1.45 ± 0.54	0.84 ± 0.30	30.0% ± 7.3%	24.5% ± 6.8%	1.73 ± 0.88	0.00 ± 0.00

*Surgical patients who had histopathologic diagnosis.
N = nodule; T = thyroid.

significant difference was found between WON and WOT in Groups A ($p < 0.01$) and B ($p < 0.001$).

Figures 1, 2 and 3 show the scintigraphic pattern of each group. Table 1 shows individual results for Group A and B patients.

Cytologic Data

Ten specimens had inadequate results (Group A = 1; Group B = 5; Group C = 4). An abundant quantity of oncocytarian cells was found only in Group A; five nodules in Group B and 14 in Group C proved to be benign. In Group B, two nodules displayed suspected malignancy and three were malignant.

Histopathologic Data

Histopathology was performed on five patients in Group A, ten in Group B and on five in Group C. In Group A patients, a Hürthle cell tumor was diagnosed (two carcinoma and three adenoma). Oxyphilic cellularity ranged from 50% to 100%. In Group B patients, hystopathology revealed colloid cysts (n = 1), papillary carcinoma (n = 4) and follicular carcinoma (n = 5). In Group C patients, colloid nodules (n = 2) and follicular adenoma (n = 3) were diagnosed. Oxyphilic cellularity was not observed in any Group B or C patients.

DISCUSSION

Thyroid nodularity is a common finding. Fortunately, the rate of malignancy is relatively low, representing 5%–6.5% of all nodules (*22,23*). The diagnosis of thyroid cancer challenges specialists in various fields. Most investigators stress the importance of thyroid sonography in differentiating benign from malignant nodules on the basis of their ultrasound features (*5,6*). Although a hypoechoic lesion is more likely to be malignant than benign, malignancy was found only in 63% of lesions, whereas 4% of hyperechoic lesions, more likely to be benign, were malignant (*7*). Thyroid aspiration and biopsy are widely accepted techniques for assessing nodules. These techniques require expertise in obtaining, preparing and interpreting the specimen (*2*), and experienced centers are able to get adequate specimens from 90% to 97% of patients (*3,4*). Thyroid scintigraphy with ^{201}Tl, a potassium analog tracer, did not lead to conclusive results. In a group of 76 patients who had undergone surgery, Ochi et al. (*8*) found intense uptake in the early images and retention in the late images in 35/37 malignant and in 4/39 benign nodules using a visual scoring method. This promising pattern for differentiating between benign and malignant nodules was not confirmed

by others. Henze et al. (*11*) found a sensitivity of 60% and a specificity of 93% and Bleichrodt et al. (*9*) found sensitivities and specificities of 25% and 95%, respectively, for detecting malignancy. Since visual interpretation of ^{201}Tl uptake may be inconclusive in detecting malignancy, Hardoff et al. (*10*) suggested early and late lesion-to-nonlesion ratios. They found a sensitivity of 100% and specificity of 62%. In their series, one patient with Hürthle cell adenoma was included in the intense uptake group in the early image with fading activity in the late image.

MIBI has also been reported to localize in several tumors. We believe that MIBI is potentially superior to ^{201}Tl for thyroid imaging because of the optimal physical properties of ^{99m}Tc, its higher count rate and higher lesion-to-background ratio. In a series of 34 surgically diagnosed nodules, Földes et al. (*17*) found that dual-phase MIBI scintigraphy was not specific for thyroid malignancy; the late image was obtained 1 hr postinjection. We partially agree with this finding. In fact, we found that double-phase scintigraphy with MIBI correctly identified patients with Hürthle cell tumors showing persistent tracer uptake on the late image in contrast with other tumors; some of which showed intense uptake with washout and others which did not show any tracer uptake.

CONCLUSION

The Hürthle cell tumor is a neoplasm composed exclusively or predominantly of follicular cells exhibiting oxyphilic features due to the presence of abundant granular acidophilic cytoplasm which is represented by crowded mitochondria and is responsible for MIBI uptake (*24–26*). Controversy arises from the view that all Hürthle cell tumors are malignant (carcinoma) or potentially malignant (adenoma); thus total thyroidectomy is suggested as the treatment of choice (*27,28*). The fact that the adenoma undergoes malignant transformation (*1*) and the carcinoma may spread to the lymph nodes and metastatize in the lungs lends support for this treatment option. Moreover, Hürthle cell carcinoma has a higher morbidity and mortality and usually does not concentrate radioiodine (*27,29–35*), except in a minority of local recurrencies or metastases (*36–38*). Because of this, correct diagnosis of such tumors is important and our data are promising in this regard. In fact, persistent MIBI uptake seems to be characteristic of the Hürthle cell tumor. Unfortunately, reactive oxyphilic cells are present in benign goiters and in chronic thyroiditis (*27,28,39*), which may limit the method's specificity. Since we did not observe benign nodules with oxyphil cells, additional data are needed to confirm our findings.

REFERENCES

1. McDonald RJ, Wu S, Jensen JL, et al. Malignant transformation of a Hürthle cell tumor: case report and survey of the literature. *J Nucl Med* 1991;32:1266–1269.
2. Ross DS. Evaluation of the thyroid nodule. *J Nucl Med* 1991;32:2181–2192.
3. Nishiyama RH, Bigos ST, Goldfarb WB, et al. The efficacy of simultaneous fine-needle aspiration and large-needle biopsy of the thyroid gland. *Surgery* 1986;100:1133–1137.
4. Hall TL, Layfield LJ, Philippe A, et al. Sources of diagnostic error in fine needle aspiration of the thyroid. *Cancer* 1989;63:718–725.
5. Molitch ME, Beck JR, Dreisman M, et al. The cold thyroid nodule: an analysis of diagnostic and therapeutic options. *Endocrinol Rev* 1984;5:185–199.
6. Van Herle AJ, Rich P, Ljung BME, et al. The thyroid nodule. *Ann Intern Med* 1982;96:221–232.
7. Solbiati L, Volterrani L, Rizzato G, et al. The thyroid gland with low uptake lesions: evaluation by ultrasound. *Radiology* 1985;155:187–191.
8. Ochi H, Sawa H, Fukuda T, et al. Thallium-201-chloride thyroid scintigraphy to evaluate benign and/or malignant nodules. *Cancer* 1982;50:236–240.
9. Bleichrodt RP, Vermey A, Piers A, et al. Early and delayed thallium-201 imaging. Diagnosis of patients with cold thyroid nodules. *Cancer* 1987;60:2621–2623.
10. Hardoff R, Baron E, Sheinfeld M. Early and late lesion-to-nonlesion ratio of thallium-201-chloride uptake in the evaluation of "cold" thyroid nodules. *J Nucl Med* 1991;32:1873–1876.
11. Henze E, Roth J, Boerer H, et al. Diagnostic value of early and delayed Tl-201 thyroid scintigraphy in the evaluation of cold nodules for malignancy. *Eur J Nucl Med* 1986;211:413–416.
12. Taillefer R, Lambert R, Dupras G, et al. Clinical comparison between ^{201}Tl and ^{99m}Tc methoxy isobutyl isonitrile (hexamibi) myocardial perfusion imaging for detection for coronary artery disease. *Eur J Nucl Med* 1989;15:280–286.
13. Iskandrian A, Heo J, Kong B, et al. Use of technetium-99m-isonitrile (RP-30A) in assessing left ventricular perfusion and function at rest and during exercise in coronary artery disease and comparison with coronary arteriography and exercise thallium-201 SPECT images. *Am J Cardiol* 1989;64:270–275.
14. Kiat H, Maddahi J, Roy L, et al. Comparison of technetium-99m-methoxy-isobutyl-isonitrile and thallium-201 for evaluation of coronary artery disease by planar and tomographic methods. *Am Heart J* 1989;117:1–11.
15. Watson RG, Brennan MD, Goelpner JRj, et al. Invasive Hürthle cell carcinoma of the tyroid: natural history and management. *Mayo Clin Proc* 1984;59:851–855.
16. Vattimo A, Bertelli P, Favilli R, et al. Myocardial imaging with ^{99m}Tc-Methoxyisobutylisonitrile in the assessment of reperfusion after intravenous thrombolytic treatment for acute myocardial infarction. *Nuc Compact* 1989;20:117–120.
17. Földes I, Lèvay A, Stotz G. Comparative scanning of thyroid nodules with technetium-99m pertecnetate and technetium-99m methoxyisobutylisonitrile. *Eur J Nucl Med* 1993;20:330–333.
18. Vattimo A, Bertelli P, Burroni L. Effective visualization of suppressed thyroid tissue by means of baseline Methoxy-isobutyl-isonitrile in comparison with ^{99m}Tc pertechnetate scintigraphy after TSH stimulation. *J Nucl Biol Med* 1992;36:315–318.
19. Taillefer R, Boucher Y, Potvin C, et al. Detection and localization of parathyroid adenomas in patients with hyperparathyroidism using a single radionuclide imaging procedure with technetium-99m-sestamibi (double-phase study). *J Nucl Med* 1992;23:1801–1807.
20. Vattimo A, Bertelli P, Burroni L, et al. Single injection-dual phase scintigraphy with ^{99m}Tc-MIBI versus dual isotope (^{201}Tl-^{99m}Tc-pertechnetate) study in the preoperative assessment of parathyroid adenoma. *J Nucl Biol Med* 1994;38:374–375.
21. Geatti O, Shapiro B, Orsolon PG, et al. Localization of parathyroid enlargement: experience with technetium-99m methoxy isobutyl isonitrile and thallium-201 scintigraphy, ultrasonography and computed tomography. *Eur J Nucl Med* 1994;21:17–22.
22. Werk EE, Vernon BM, Gonzalez JJ, et al. Cancer in thyroid nodules. A community hospital survey. *Arch Intern Med* 1984;144:474–476.
23. Belfiore A, Giuffrida D, La Rosa GL, et al. High frequency of cancer in cold thyroid nodules occurring at young age. *Acta Endocrinol* 1989;121:197–202.
24. Carvalho PA, Chiu ML, Kronauge JF, et al. Subcellular distribution and analysis of technetium-99m-MIBI in isolated perfused rat hearts. *J Nucl Med* 1992;33:1516–1521.
25. Piwnica-Worms D, Kronauge JF, Chiu ML. Uptake and retention of hexakis (2-methoxyisobutylisonitrile) technetium (I) in cultured chick myocardial cells: mitochondrial and plasma membrane potential-dependence. *Circulation* 1990;82:1826–1838.
26. Chiu ML, Kronauge JF, Piwnica-Worms D. Effect of mitochondrial and plasma membrane potentials on accumulation of hexakis (2-methoxyisobutylisonitrile) technetium (I) in cultured mouse fibroblasts. *J Nucl Med* 1990;31:1646–1653.

27. Gundry SR, Burney RE, Thompson NW, et al. Total thyroidectomy for Hürthle cell neoplasm of the thyroid. *Arch Surg* 1983;118:529–532.
28. Thompson NW, Dunn EL, Batsakis JG, et al. Hürthle cell lesions of the thyroid gland. *Surg Gynecol Obstet* 1974;139:555–560.
29. Rossi RL, Nieroda C, Cady B, et al. Malignancies of the thyroid gland: the Lahey clinic experience. *Surg Clin N Am* 1985;65:211–230.
30. Har-El G, Hadar T, Levy R, et al. Hürthle cell carcinoma of the thyroid gland: a tumor of moderate malignancy. *Cancer* 1986;57:1613–1617.
31. Krishnamurthy GT, Blahd WH. Radioiodine I-131 therapy in the management of thyroid cancer: a prospective story. *Cancer* 1977;40:195–202.
32. Frazell EL, Duffy BR. Hürthle cell cancer of the thyroid: a review of 40 cases. *Cancer* 1951;4:952–956.
33. Tollefsen HR, Shah JP, Huvos AG. Hürthle cell carcinoma of the thyroid. *Am J Surg* 1975;130:390–394.
34. McLeod MK. Hürthle cell neoplasm of the thyroid. *Otolar Clin NA* 1990; 23:441–452.
35. Samaan NA, Shultz PN, Haynie TP, et al. Pulmonary matastasis of differentiated thyroid carcinoma: treatment results in 101 patients. *J Clin Endocrinol Metab* 1985;60:376–380.
36. Hamann A, Gratz K, Soudah B, et al. Szintigraphie mit 131-J bei oxyphilen Karzinomen der Schilddrüse. *Nuklearmedizin* 1994;33:219–223.
37. Vergara E, Lastoria S, Varella P, et al. Technetium-99m-pentavalent dimercaptosuccinic acid uptake in Hürthle cell tumor of the thyroid. *J Nucl Biol Med* 1993;37:65–68.
38. Yen T, Lin H, Lee C, et al. The role of technetium-99m sestamibi whole body scans in diagnosing metastatic Hürthle cell carcinoma of the thyroid gland after total thyroidectomy: a comparison with iodine-131 and thallium-201 whole-body scans. *Eur J Nucl Med* 1994;21:980–983.
39. Miller RH, Estrada R, Sneed WF, et al. Hürthle cell tumors of the thyroid gland. *Laryngoscope* 1983;93:884–886.

(continued from page 9A)

FIRST IMPRESSIONS

FIGURE 1. A posterior view bone scan depicts a large doughnut lesion in the skull.

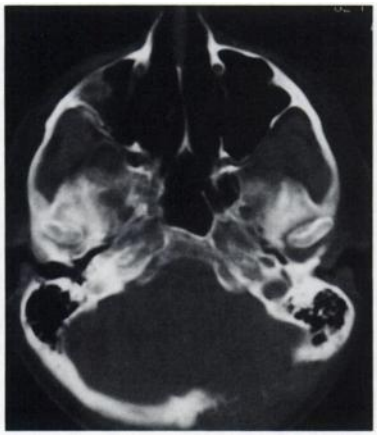

FIGURE 2. Brain CT scan of depicts a large lytic lesion in the skull.

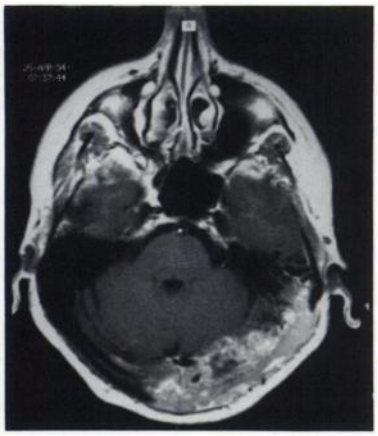

FIGURE 3. Brain MR image depicts a bony metastatic lesion.

PURPOSE

A 62-yr-old woman with breast cancer diagnosed in 1992. She has had a left mastectomy. There was no lymph node involvement at that time. She was doing well until she started to experience headaches, which were getting worse over the past 2 wk and accompanied by visual symptoms. A bone scan was obtained, which revealed a large doughnut lesion in the left posterior parietal and occipital regions of the skull, crossing to the right occipital bone (Fig. 1). Multiple lesions also were seen in the ribs, spine, pelvis and left humerus. A CT scan of the head confirmed a large lytic lesion in the skull (Fig. 2). Brain MRI revealed a bony metastatic lesion, with extensive dural involvement as well as parenchymal, dural venous sinuses and left mastoid air cells and bone involvement (Fig. 3).

TRACER

Technetium-99m-MDP (800 MBq)

ROUTE OF ADMINISTRATION

Intravenous injection

TIME AFTER INJECTION

Three minutes

INSTRUMENTATION

Large field of view gamma camera with a low-energy, all-purpose collimator

CONTRIBUTOR

S.K. Ghali, St. Joseph's Health Centre, London, Ontario, Canada